

# The Geometry of Hidden Modes in Distance-Based Formation Control\*

Solomon Goldgraber Casspi\* Daniel Zelazo\*

\* Stephen B. Klein Faculty of Aerospace Engineering, Technion - Israel Institute of Technology, Haifa, Israel (e-mail: solomon.g@campus.technion.ac.il, dzelazo@technion.ac.il).

**Abstract:** This paper presents a geometric input-output analysis of hidden modes in distance-based formation control. We study the linearized dynamics under a gradient control law to characterize the system's structural limitations and their dynamic consequences. Our main contribution is a unified geometric framework for uncontrollable modes. We first prove that uncontrollable rigid-body modes are pure rotations about the input node, defining a global rotational subspace  $\mathcal{R}_i$ . To generalize this, we introduce the local rotational subspace,  $\mathcal{T}_i$ , which contains all motions, including deformations, that are locally invisible to the controller at node  $i$ . These two geometric objects provide a complete decomposition of the uncontrollable subspace. Finally, we demonstrate the dynamic implications of this structure by proving that the system's ability to recover its shape is determined by an input's alignment with the local component of the standard rotational rigid-body mode, directly linking the geometry of hidden modes to disturbance rejection. We illustrate our results with a case study.

**Keywords:** Multi-agent systems, Formation control, Control over networks, Controllability.

## 1. INTRODUCTION

The coordination of multi-agent systems (MASs) is a cornerstone of modern engineering, enabling applications from satellite formation flying to drone swarms and robotic teams (Chung et al. (2018)). A fundamental task in this domain is formation control, where agents must achieve and maintain a specific geometric pattern. In many real-world scenarios, such as indoor or underwater environments, global positioning is unavailable, forcing agents to rely on local, relative sensing. Distance-based formation control, where the desired shape is defined by a set of inter-agent distances, provides a robust and decentralized solution for such settings (Oh and Ahn (2011)).

A standard approach to this problem employs a gradient-based control law, where each agent adjusts its motion to minimize the error in its local distance measurements (Krick et al. (2009)). While the stability and convergence properties of these controllers are well-understood Oh et al. (2015), their dynamic performance under external disturbances remains an open area of investigation. How does a localized disturbance, such as a wind gust affecting a single drone, propagate through the formation? How do the placement of actuators and sensors and the geometry of the formation itself affect the system's ability to reject such disturbances? To answer these questions, a formal input-output modeling framework is required.

The analysis of controllability and observability in networked systems has a rich history, particularly for linear consensus-type dynamics. Foundational work has established deep connections between a network's controllability

and its underlying graph topology, including the role of graph symmetries Rahmani et al. (2009) and the placement of leader agents Tanner (2004). However, these classical results are often tailored to systems with simple, unweighted graph Laplacians. They do not directly address the challenges posed by distance-based formation control, where the system dynamics are governed by a configuration-dependent, weighted Laplacian that introduces geometric constraints and nonlinearities.

This paper develops such a framework to analyze the input-output properties of distance-based formations. We begin by linearizing the nonlinear gradient dynamics around a target equilibrium configuration. This yields a linear time-invariant (LTI) model whose system matrix is a configuration-dependent, weighted graph Laplacian. This model, while an approximation, allows us to leverage the powerful tools of classical systems theory to analyze the formation's controllability and observability.

The main contributions of this paper are twofold. First, we develop a unified geometric framework that provides a complete decomposition of the uncontrollable subspace. We define the global rotational subspace,  $\mathcal{R}_i$ , to characterize uncontrollable rigid-body modes, and the local rotational subspace,  $\mathcal{T}_i$ , to characterize locally hidden deformations. Second, we analyze the dynamic implications of this structure, demonstrating that the system's ability to recover its shape is determined by the alignment of a disturbance with the local component of the standard rotational rigid-body mode. This establishes a direct link between the geometry of hidden modes and disturbance rejection.

\* This work was supported by the Israel Science Foundation grant no. 453/24 and the Gordon Center for Systems Engineering.

The remainder of this paper is organized as follows. Section 2 provides the necessary background on rigidity theory and system-theoretic concepts. Section 3 formally defines the problem, introducing the nonlinear dynamics and the linearized model used for analysis. Section 4 presents our main theoretical contribution: a complete geometric characterization of the uncontrollable subspace. Finally, Section 5 analyzes the dynamic implications of this geometric structure and illustrates the results with a case study.

*Notations* Throughout,  $I_d$  denotes the identity matrix in  $\mathbb{R}^d$ ,  $e_k$  is the  $k$ -th standard basis vector in  $\mathbb{R}^n$ , and  $\Omega$  denotes a  $d \times d$  skew-symmetric matrix representing an infinitesimal rotation. For  $d = 2$ , this is uniquely represented (up to a scalar) by  $\Omega = \begin{pmatrix} 0 & -1 \\ 1 & 0 \end{pmatrix}$ . The Kronecker product is denoted by  $\otimes$ . For a stacked vector  $v \in \mathbb{R}^{nd}$ , its component corresponding to agent  $i$  is denoted  $v_i \in \mathbb{R}^d$ . The standard Euclidean inner product is denoted by  $\langle \cdot, \cdot \rangle$ .

## 2. PRELIMINARIES

This section provides the necessary background on graph rigidity and system-theoretic concepts that form the basis of our analysis.

### 2.1 Rigidity of Graphs

A formation of  $n$  agents is modeled as a *framework*  $(\mathcal{G}, p)$ , where  $\mathcal{G} = (\mathcal{V}, \mathcal{E})$  is an undirected graph with a vertex set  $\mathcal{V} = \{1, \dots, n\}$  and an edge set  $\mathcal{E}$  of size  $m = |\mathcal{E}|$ . The vector  $p \in \mathbb{R}^{nd}$  is the stacked vector of agent positions. A reference configuration, used to define the desired inter-agent distances, is denoted  $p^*$ .

The shape of the framework is encoded by the vector of squared inter-agent distances, known as the *rigidity function*,  $r(p) : \mathbb{R}^{nd} \times \mathcal{G} \rightarrow \mathbb{R}^m$ , with

$$[r(p)]_k = \|p_i - p_j\|^2, \quad \text{for each edge } k = (i, j) \in \mathcal{E}. \quad (1)$$

The first-order change in these distances due to an infinitesimal motion  $v \in \mathbb{R}^{nd}$  about the reference configuration  $p^*$  is given by the Taylor expansion  $r(p^* + tv) - r(p^*) = tR(p^*)v + o(t^2)$ , where the Jacobian  $R(p^*) := \nabla_p r(p)|_{p=p^*}$  is the *rigidity matrix* evaluated at  $p^*$ .

An infinitesimal motion  $v$  that preserves all edge lengths to first order is called an *infinitesimal flex*, and must satisfy  $R(p^*)v = 0$ . The set of all such flexes forms the nullspace  $\ker(R(p^*))$ . Any *rigid body motion* (RBM) of the entire framework is a trivial infinitesimal flex - these are the rotations and translations of the configuration. A framework is *infinitesimally rigid* if the only infinitesimal flexes are the RBMs, meaning the nullspace of the rigidity matrix is precisely the space of infinitesimal RBMs. For a generic framework in  $\mathbb{R}^2$ , this is equivalent to the rank condition  $\text{rank}(R(p^*)) = 2n - 3$ .

The rigidity matrix also defines two other fundamental subspaces. The nullspace of its transpose,  $\ker(R(p^*)^\top)$ , is the space of *self-stresses*. A non-zero self-stress is a set of tensions and compressions on the edges that self-equilibrate at every node. By the fundamental theorem of linear algebra, the image of the transpose,  $\text{Im}(R(p^*)^\top)$ ,

is the orthogonal complement to the space of RBMs. It therefore represents the space of all infinitesimal *deformations*. For a comprehensive treatment of rigidity theory, see Asimow and Roth (1979); Connelly (2005).

### 2.2 Controllability and Observability of LTI Systems

Consider a general LTI system  $\dot{x} = Ax + Bu$ ,  $y = Cx$ . The system's controllability and observability properties determine which internal modes can be influenced by the input or seen at the output. A key tool for this analysis is the Popov-Belevitch-Hautus (PBH) test. For a mode of the system represented by an eigenvector  $v$  of  $A$ , the PBH test provides a direct algebraic condition:

- i) The mode  $v$  is *uncontrollable* if and only if it lies in the nullspace of  $B^\top$ , i.e.,  $B^\top v = 0$ .
- ii) The mode  $v$  is *unobservable* if and only if it lies in the nullspace of  $C$ , i.e.,  $Cv = 0$ .

These conditions allow for a formal decomposition of the state space into four fundamental subspaces. We denote the controllable subspace as  $\mathcal{C}$  and the observable subspace as  $\mathcal{O}$ . Their orthogonal complements, the uncontrollable and unobservable subspaces, are denoted  $\overline{\mathcal{C}}$  and  $\overline{\mathcal{O}}$ , respectively. Any eigenvector  $v$  can be classified based on its membership in the intersection of these subspaces:

- *Controllable and observable*:  $v \in \mathcal{C} \cap \mathcal{O}$ .
- *Uncontrollable but observable*:  $v \in \overline{\mathcal{C}} \cap \mathcal{O}$ .
- *Controllable but unobservable*:  $v \in \mathcal{C} \cap \overline{\mathcal{O}}$ .
- *Uncontrollable and unobservable*:  $v \in \overline{\mathcal{C}} \cap \overline{\mathcal{O}}$ .

A mode that is not both controllable and observable is often called a *hidden mode* (Skogestad and Postlethwaite (2005)).

## 3. PROBLEM FORMULATION

We consider a formation of  $n$  agents in  $\mathbb{R}^d$  (typically  $d = 2$ ) with single-integrator dynamics,  $\dot{p}_i = u_i$ , a standard model in the distance-based formation control literature (Krick et al. (2009); Oh and Ahn (2011); Babazadeh and Selmic (2019)). The agent interactions are described by an undirected sensing graph  $\mathcal{G}$ .

The control objective is to steer the formation to a configuration  $p$  that satisfies a desired set of inter-agent distances, defined by a reference configuration  $p^*$ . This is achieved using a standard gradient-descent control law. We define a potential function based on the collective error in squared edge lengths:

$$V(p) = \frac{1}{2} \|r(p) - r(p^*)\|^2, \quad (2)$$

where  $r(p)$  is the rigidity function defined (1). The control law is the negative gradient of this potential,  $\dot{p} = -\nabla_p V(p)$ , which is a standard approach in the literature (see, e.g., Krick et al. (2009); Olfati-Saber and Murray (2002); Oh et al. (2015)). This yields the closed-loop dynamics:

$$\dot{p} = -R(p)^\top (r(p) - r(p^*)). \quad (3)$$

To analyze the system's response to external disturbances, we augment these dynamics to create an input-output model. To build intuition, we focus on the case of a single

actuated agent  $i$  and a single measured agent  $j$ . The nonlinear input-output model is:

$$\dot{p} = -R(p)^\top(r(p) - r(p^*)) + Bw, \quad (4)$$

$$y = Cp, \quad (5)$$

where  $w \in \mathbb{R}^d$  and the input and output matrices are  $B = e_i \otimes I_d$  and  $C = e_j^\top \otimes I_d$ .

Direct analysis of the nonlinear model (4) is challenging. To gain tractable insights, we linearize the system around the equilibrium point  $(p^*, w = 0)$ . Letting  $\delta p = p - p^*$ , the first-order Taylor expansion of the dynamics yields the LTI model:

$$\delta\dot{p} = A\delta p + B\delta w, \quad \delta y = C\delta p, \quad (6)$$

where the system matrix  $A$  is the weighted graph Laplacian, or "stiffness matrix," given by:

$$A = -R(p^*)^\top R(p^*). \quad (7)$$

This LTI model forms the basis of our system-theoretic analysis in the following sections.

#### 4. GEOMETRIC CHARACTERIZATION OF HIDDEN MODES

This section develops a geometric characterization of the hidden modes for the linearized system (6). We first establish their existence and algebraic structure before revealing their geometric form.

##### 4.1 Algebraic Foundations of Hidden Modes

We begin by establishing that for an infinitesimally rigid formation, hidden modes are an unavoidable consequence of using a single actuator.

*Proposition 1.* (Existence of Hidden RBMs). Consider the linearized system (6) for an infinitesimally rigid framework in  $\mathbb{R}^d$  with  $d \geq 2$ , actuated at a single node  $i$ . Let  $\bar{\mathcal{C}}$  be the uncontrollable subspace and  $E_0 = \ker(R(p^*))$  be the RBM eigenspace. Then the dimension of the uncontrollable RBM subspace satisfies

$$\dim(\bar{\mathcal{C}} \cap E_0) \geq \frac{d(d-1)}{2}.$$

Since  $d \geq 2$ , this guarantees the existence of at least one uncontrollable RBM.

**Proof.** The RBM eigenspace  $E_0$  corresponds to the zero-eigenspace of the system matrix  $A = -R(p^*)^\top R(p^*)$ . For an infinitesimally rigid framework in  $\mathbb{R}^d$ , this space has dimension  $\dim(E_0) = d(d+1)/2$ . By the PBH test, the uncontrollable subspace is  $\bar{\mathcal{C}} = \bigoplus_{\lambda} (E_\lambda \cap \ker(B^\top))$ . The uncontrollable part of the RBM eigenspace is therefore  $E_0 \cap \ker(B^\top)$ . The dimension of this subspace is given by:

$$\begin{aligned} \dim(E_0 \cap \ker(B^\top)) &\geq \dim(E_0) - \text{rank}(B) \\ &= \frac{d(d+1)}{2} - d = \frac{d(d-1)}{2}. \end{aligned}$$

For any  $d \geq 2$ , we have  $d(d-1)/2 \geq 1$ , which proves the existence of at least one uncontrollable RBM.  $\square$

Having established their existence, we now seek to understand their structure.

*Proposition 2.* (Uncontrollable Subspace Decomposition).

The total uncontrollable subspace  $\bar{\mathcal{C}}$  can be decomposed into its RBM and deformational components as:

$$\bar{\mathcal{C}} = (\ker(R(p^*)) \cap \ker(B^\top)) \oplus (\text{Im}(R(p^*)^\top) \cap \ker(B^\top)), \quad (8)$$

where  $\ker(R(p^*))$  is the RBM subspace and  $\text{Im}(R(p^*)^\top)$  is the subspace of shape-changing deformations.

**Proof.** The proof follows from the spectral properties of the symmetric matrix  $-R(p^*)^\top R(p^*)$ . The eigenspace for  $\lambda = 0$  is  $E_0 = \ker(R(p^*))$ , and the direct sum of all other eigenspaces is  $\bigoplus_{\lambda \neq 0} E_\lambda = \text{Im}(R(p^*)^\top)$ . Since these two subspaces are orthogonal, the total uncontrollable subspace can be partitioned as:

$$\begin{aligned} \bar{\mathcal{C}} &= (E_0 \cap \ker(B^\top)) \oplus \left( \bigoplus_{\lambda \neq 0} (E_\lambda \cap \ker(B^\top)) \right) \\ &= (\ker(R(p^*)) \cap \ker(B^\top)) \oplus (\text{Im}(R(p^*)^\top) \cap \ker(B^\top)), \end{aligned}$$

where the second equality holds because the intersection distributes over the direct sum of orthogonal subspaces.  $\square$

This decomposition provides the algebraic foundation. To find a geometric interpretation for each term in (8), we use the PBH test, which states that an eigenvector  $v$  of  $A$  is uncontrollable if and only if  $B^\top v = 0$ . For our single-actuator system with  $B = e_i \otimes I_d$ , this condition simplifies to a direct "pinning" constraint at the agent level.

*Lemma 3.* (Pinning Constraint). An eigenvector  $v$  is uncontrollable from an input applied at agent  $i$  if and only if its component at that agent vanishes, i.e.,  $v_i = 0$ . Likewise,  $v$  is unobservable from an output measured at agent  $j$  if and only if  $v_j = 0$ .

**Proof.** From the PBH test, a mode  $v$  is uncontrollable if and only if  $B^\top v = 0$ . For a single actuator at node  $i$ , the input matrix is  $B = e_i \otimes I_d$ . The condition becomes:

$$B^\top v = (e_i^\top \otimes I_d)v = v_i = 0.$$

The proof for the unobservable case is dual, with  $C = e_j^\top \otimes I_d$ .  $\square$

##### 4.2 Geometric Characterization of the Uncontrollable RBM

We now use pinning constraint formulated in Lemma 3 to find a geometric interpretation for the RBM and deformational components of the uncontrollable subspace. We first ask: what is the geometric form of the guaranteed hidden RBM from Proposition 1? Applying the pinning constraint to a general RBM reveals its structure.

*Proposition 4.* (Uncontrollable RBM is a Pure Rotation). The uncontrollable RBM subspace,  $\ker(R(p^*)) \cap \ker(B^\top)$ , is the  $d(d-1)/2$ -dimensional rotational subspace  $\mathcal{R}_i(p^*)$ . This subspace consists of all infinitesimal motions corresponding to a pure rotation of the framework about the actuator node  $i$ ,

$$\mathcal{R}_i(p^*) := \{v \in \mathbb{R}^{dn} \mid v_k = \Omega(p_k^* - p_i^*), \forall k \in \mathcal{V}\},$$

as illustrated in Figure 1.

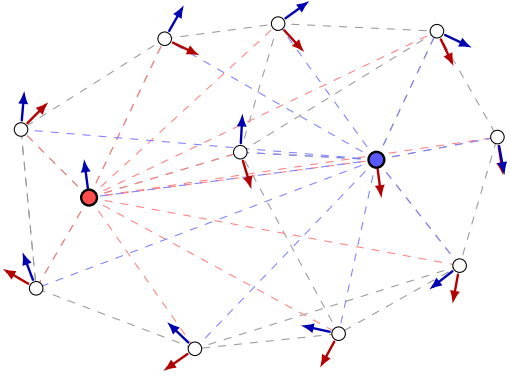


Fig. 1. Geometric interpretation of the hidden RBM subspaces, illustrated for the planar case ( $d = 2$ ). The dashed gray lines show the framework's configuration for visual context. The red arrows depict a motion in the uncontrollable rotational subspace  $\mathcal{R}_i(p^*)$ , a pure rotation of the *entire* framework about the actuated node  $i$  (red). The dashed red lines emphasize that this global rotation depends on the relative position of every node with respect to node  $i$ . Similarly, the blue arrows and dashed lines illustrate a motion in the unobservable rotational subspace  $\mathcal{R}_j(p^*)$ , a pure rotation about the measured node  $j$  (blue).

**Proof.** An arbitrary RBM  $v \in \ker(R(p^*))$  can be uniquely decomposed into a translation and a rotation about the center of mass,  $p_{\text{cm}} = \frac{1}{n} \sum_k p_k^*$ . The motion at agent  $k$  is given by

$$v_k = b + [v_r]_k,$$

where  $b \in \mathbb{R}^d$  is the translational velocity and  $[v_r]_k = \Omega(p_k^* - p_{\text{cm}})$  is the local velocity of the rotational mode at node  $k$ . The uncontrollability condition from Lemma 3 requires the motion at the actuated agent  $i$  to be zero,  $v_i = 0$ . This imposes a constraint on the translation,

$$b + [v_r]_i = 0 \implies b = -[v_r]_i = -\Omega(p_i^* - p_{\text{cm}}).$$

This fixes the translational component in terms of the rotational component. Substituting this expression for  $b$  back into the general motion for an arbitrary agent  $k$  yields

$$\begin{aligned} v_k &= -[v_r]_i + [v_r]_k \\ &= -\Omega(p_i^* - p_{\text{cm}}) + \Omega(p_k^* - p_{\text{cm}}) \\ &= \Omega(p_k^* - p_i^*). \end{aligned}$$

This resulting motion vector  $v$ , whose components are  $v_k = \Omega(p_k^* - p_i^*)$ , is precisely the form of an element in the rotational subspace  $\mathcal{R}_i(p^*)$  as defined in the proposition.  $\square$

This proof reveals a key geometric insight: the algebraic “pinning constraint”  $v_i = 0$  forces the center of rotation of any hidden RBM to coincide with the actuated node  $i$ . This establishes a direct and intuitive link between the placement of the actuator and the geometric form of the resulting uncontrollable mode. By duality, any unobservable RBM must be a pure rotation about the measured node  $j$ . This result provides the geometric identity for the first component of the uncontrollable subspace decomposition in (8).

### 4.3 Locally Hidden Deformations

Having characterized the hidden RBMs, we now generalize our approach to find hidden deformations. The gradient controller at node  $i$  is driven only by errors in its incident edges. A motion is therefore “locally hidden” from the controller at node  $i$  if it generates no first-order change in these local edge lengths.

To formalize this, we consider the components of the rigidity function,  $[r(p)]_k = \|p_i - p_j\|^2$ , corresponding to the edges incident to node  $i$ . These form the *star relations* at  $i$ . The first-order change in these relations due to an infinitesimal motion  $v$  is given by

$$\delta[r(p)]_k = 2(p_i^* - p_j^*)^\top (v_i - v_j), \text{ for each edge } k = (i, j) \in \mathcal{E}.$$

A motion  $v$  is locally hidden from node  $i$  if it produces no change in these local measurements, i.e.,  $\delta[r(p)]_k = 0$  for all edges  $k$  incident to  $i$ . This motivates the following definition, which adds the pinning constraint  $v_i = 0$ .

**Definition 5.** (The Local Rotational Subspace  $\mathcal{T}_i$ ). The set of infinitesimal motions that fix node  $i$  and preserve the lengths of all its incident edges to first order, denoted  $\mathcal{T}_i(\mathcal{G}, p^*)$ , is defined as

$$\mathcal{T}_i := \{v \in \mathbb{R}^{dn} : v_i = 0 \text{ and } (p_k^* - p_i^*)^\top v_k = 0, \forall (i, k) \in \mathcal{E}\}.$$

This subspace is spanned by a set of vectors corresponding to *elementary rotational motions*. Each basis vector, denoted  $\tau_{i \rightarrow k}$ , represents a motion where only a single neighbor  $k$  rotating infinitesimally around the fixed central node  $i$ . Such a motion has the form:

$$\tau_{i \rightarrow k} := (e_k \otimes I_d) \Omega (p_k^* - p_i^*).$$

These elementary motions are illustrated in Figure 2.

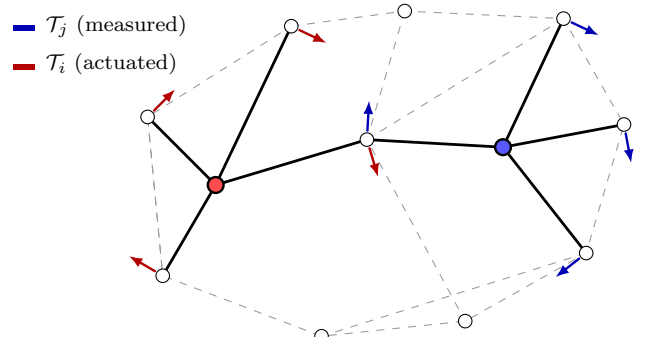


Fig. 2. Geometric interpretation of the local rotational subspaces, illustrated for the planar case ( $d = 2$ ). The union of the thick black and dashed gray lines represents the edges of the sensing graph  $\mathcal{G}$ . The thick black lines emphasize the star of edges incident to the actuated node  $i$  (red) and the measured node  $j$  (blue). The local rotational subspace  $\mathcal{T}_i$  is defined by these incident edges at  $i$ . The red arrows show elementary motions in  $\mathcal{T}_i$ , which are locally invisible to the controller at  $i$ . Similarly, the blue arrows show motions in  $\mathcal{T}_j$ , which are locally invisible to the measurement at  $j$ . Each arrow is orthogonal to its corresponding edge vector, representing a purely rotational motion of a neighbor around its central node.

**Proposition 6.** (Geometric Subspace Inclusion). The rotational subspace  $\mathcal{R}_i(p^*)$  is a subspace of the local rotational subspace  $\mathcal{T}_i(G, p^*)$ ,

$$\mathcal{R}_i(p^*) \subseteq \mathcal{T}_i(G, p^*).$$

**Proof.** A motion  $v \in \mathcal{R}_i(p^*)$  has the form  $v_k = \Omega(p_k^* - p_i^*)$  for some skew-symmetric matrix  $\Omega$ . This motion satisfies the first condition of Definition 5,  $v_i = \Omega(p_i^* - p_i^*) = 0$ . It also satisfies the second condition,  $(p_k^* - p_i^*)^\top v_k = (p_k^* - p_i^*)^\top \Omega(p_k^* - p_i^*) = 0$ , which holds for any vector because  $\Omega$  is skew-symmetric. Thus, any element of  $\mathcal{R}_i(p^*)$  is also an element of  $\mathcal{T}_i(G, p^*)$ .  $\square$

The inclusion  $\mathcal{R}_i(p^*) \subseteq \mathcal{T}_i(G, p^*)$  highlights a key distinction. A motion is “locally rigid at  $i$ ” if it preserves the lengths of all edges incident to node  $i$  to first order. The global rotation in  $\mathcal{R}_i$  is one such motion, as it preserves all edge lengths. However,  $\mathcal{T}_i$  also contains motions that are not globally rigid. Consider an elementary rotational motion  $\tau_{i \rightarrow k} \in \mathcal{T}_i$ , which rotates only neighbor  $k$  around the fixed node  $i$ . This motion preserves the length of the edge  $(i, k)$  by construction, making it locally rigid at  $i$ . However, it will generally change the distances between node  $k$  and any other node in the framework, causing a global deformation. Therefore, while  $\mathcal{R}_i$  contains only a single global RBM, the local rotational subspace  $\mathcal{T}_i$  is generally larger and also contains these globally deformational motions that lie in  $\text{Im}(R(p^*))^\perp$ .

#### 4.4 Unified Geometric Decomposition

The local rotational subspace,  $\mathcal{T}_i$ , introduced in Definition 5, provides a complete and unified geometric characterization for the entire uncontrollable subspace, regardless of whether the framework is rigid or flexible.

**Theorem 7.** (Unified Geometric Characterization). For any framework  $(G, p^*)$  with a single actuator at node  $i$ , the total uncontrollable subspace  $\bar{\mathcal{C}}$  is precisely the local rotational subspace  $\mathcal{T}_i$ :

$$\bar{\mathcal{C}} = \mathcal{T}_i(G, p^*).$$

**Proof.** By the PBH test and Lemma 3, a mode is uncontrollable if and only if it is pinned at the actuator,  $v_i = 0$ . The gradient control law at node  $i$  is driven by errors in its incident edges. A motion is therefore invisible to this local control action if it preserves the lengths of all incident edges to first order. The subspace  $\mathcal{T}_i$  is, by definition, the set of all motions that satisfy both of these conditions. Therefore, it represents the entirety of the uncontrollable subspace.  $\square$

This result can be specialized to different classes of frameworks by decomposing  $\mathcal{T}_i$  based on the framework’s rigidity properties.

**Corollary 8.** (Infinitesimally Rigid Frameworks). For an infinitesimally rigid framework, the state space decomposes into orthogonal RBM and deformational subspaces,  $\mathbb{R}^{dn} = \ker(R(p^*)) \oplus \text{Im}(R(p^*))^\perp$ . The uncontrollable subspace can then be written as:

$$\bar{\mathcal{C}} = \mathcal{R}_i(p^*) \oplus (\mathcal{T}_i(G, p^*) \cap \text{Im}(R(p^*))^\perp).$$

**Proof.** For a rigid framework,  $\ker(R(p^*))$  contains only RBMs. The intersection of  $\mathcal{T}_i$  with this RBM subspace is

precisely  $\mathcal{R}_i(p^*)$  (by Prop. 4 and Prop. 6). The remainder of  $\mathcal{T}_i$  must lie in the orthogonal deformational subspace,  $\text{Im}(R(p^*))^\perp$ . The result follows from decomposing  $\mathcal{T}_i$  across these two orthogonal subspaces.  $\square$

**Corollary 9.** (Complete Graphs). For a complete graph  $G = \mathcal{K}_n$  with  $n \geq d + 1$ , the local rotational subspace is identical to the global one,  $\mathcal{T}_i(G, p^*) = \mathcal{R}_i(p^*)$ . The uncontrollable subspace simplifies to:

$$\bar{\mathcal{C}} = \mathcal{R}_i(p^*).$$

**Proof.** The condition  $n \geq d + 1$  ensures that a complete graph  $\mathcal{K}_n$  is infinitesimally rigid in  $\mathbb{R}^d$  Connely (2005). Now, let  $v$  be an arbitrary motion in  $\mathcal{T}_i(G, p^*)$ . By definition,  $v_i = 0$  and the lengths of all edges incident to node  $i$  are preserved to first order. For  $v$  to be a valid infinitesimal motion of the framework, it must preserve the lengths of all edges. Since the graph is complete, this includes the edges  $(j, k)$  for all pairs  $j, k \neq i$ . The rigidity of the framework then implies that a motion fixing one node while preserving all other inter-node distances must be a pure rigid-body rotation about the fixed node. This is precisely the definition of a motion in  $\mathcal{R}_i(p^*)$ . Thus,  $\mathcal{T}_i(G, p^*) \subseteq \mathcal{R}_i(p^*)$ . Since we already know from Prop. 6 that  $\mathcal{R}_i(p^*) \subseteq \mathcal{T}_i(G, p^*)$ , the two subspaces must be equal.  $\square$

## 5. DYNAMIC IMPLICATIONS OF HIDDEN MODES

We now analyze the dynamic consequences of the hidden modes, investigating how a localized input at agent  $i$  affects the formation’s ability to recover its shape. This reveals a direct link between the geometry of the uncontrollable subspace  $\mathcal{R}_i$  and the system’s steady-state response.

We analyze the system’s steady-state response to an impulsive input,  $w(t) = w_0\delta(t)$ , where  $w_0 \in \mathbb{R}^d$  is the direction of the impulse. The final state deviation is given by the projection of the initial impulse onto the RBM eigenspace  $E_0 = \ker(R(p^*))$ ,

$$\lim_{t \rightarrow \infty} \delta p(t) = P_0 B w_0, \quad (9)$$

where  $P_0$  is the orthogonal projection matrix onto  $E_0$ . Let  $\{v_x, v_y, v_r\}$  be an orthonormal basis for the RBM space, representing x-translation, y-translation, and rotation about the center of mass, respectively. The final state will be a linear combination of these modes,

$$\lim_{t \rightarrow \infty} \delta p(t) = c_x v_x + c_y v_y + c_r v_r, \quad (10)$$

where the coefficients are determined by the input:

$$c_x = \langle v_x, B w_0 \rangle, \quad c_y = \langle v_y, B w_0 \rangle, \quad c_r = \langle v_r, B w_0 \rangle.$$

The key insight is that shape recovery depends entirely on whether the global rotational mode  $v_r$  is excited (i.e., if  $c_r \neq 0$ ). The ability of a local input at node  $i$  to excite this global mode is determined by a simple geometric condition. The coefficient of the rotational mode in the final state is given by the inner product  $c_r = \langle v_r, B w_0 \rangle = \langle [v_r]_i, w_0 \rangle$ , where  $[v_r]_i$  is the local velocity of the rotational mode at the actuated node. This vector is a key geometric feature related to the structure of the uncontrollable subspace  $\mathcal{R}_i$ . Excitation of the rotational mode, and thus the final shape of the formation, is therefore governed by the alignment of the input direction  $w_0$  with the local vector  $[v_r]_i$ .

*Proposition 10.* (Shape Recovery Dichotomy). Consider an impulsive input  $w(t) = w_0\delta(t)$  applied at agent  $i$ . The ability of the formation to recover its shape is determined by the alignment between the input vector  $w_0$  and the local rotational vector  $[v_r]_i$ . This vector is a defining component of the uncontrollable rotational subspace  $\mathcal{R}_i$ .

(i) *Perfect Shape Recovery:*

If the input is orthogonal to the local rotational direction,  $\langle [v_r]_i, w_0 \rangle = 0$ , then the rotational mode is not excited ( $c_r = 0$ ). The resulting steady-state motion is a pure translation of the entire framework. All inter-agent distances are preserved, and the steady-state edge error is zero.

(ii) *Persistent Shape Distortion:*

If the input has a component along the local rotational direction,  $\langle [v_r]_i, w_0 \rangle \neq 0$ , then the rotational mode is excited ( $c_r \neq 0$ ). The resulting steady-state motion is a combination of translation and rotation, which causes a persistent change in the inter-agent distances and a non-zero steady-state edge error.

**Proof.** The coefficient for the rotational mode is  $c_r = \langle v_r, Bw_0 \rangle = \langle v_r, (e_i \otimes I_d)w_0 \rangle = \langle [v_r]_i, w_0 \rangle$ . We now analyze the steady-state edge error based on this coefficient. The final configuration is  $p' = p^* + \delta p(\infty)$ . An edge  $k = (j, l)$  is preserved if  $\|p'_j - p'_l\|^2 = \|p_j^* - p_l^*\|^2$ .

*Case 1: Perfect Shape Recovery* If  $c_r = 0$ , the final state is  $\delta p(\infty) = c_x v_x + c_y v_y$ . This is a pure translation, meaning the displacement is the same for all agents:  $[\delta p(\infty)]_k = b$  for some constant vector  $b \in \mathbb{R}^d$ . The new relative position for edge  $(j, l)$  is

$$p'_j - p'_l = (p_j^* + b) - (p_l^* + b) = p_j^* - p_l^*.$$

The edge lengths are perfectly preserved, resulting in zero steady-state edge error.

*Case 2: Persistent Shape Distortion* If  $c_r \neq 0$ , the final state includes a rotational component:  $[\delta p(\infty)]_k = b + c_r \Omega(p_k^* - p_{cm})$ . The new relative position for edge  $(j, l)$  is

$$\begin{aligned} p'_j - p'_l &= (p_j^* + b + c_r \Omega(p_j^* - p_{cm})) \\ &\quad - (p_l^* + b + c_r \Omega(p_l^* - p_{cm})) \\ &= (p_j^* - p_l^*) + c_r \Omega(p_j^* - p_l^*) \\ &= (I_d + c_r \Omega)(p_j^* - p_l^*). \end{aligned}$$

The new squared edge length is  $\|(I_d + c_r \Omega)(p_j^* - p_l^*)\|^2$ . For  $c_r \neq 0$ , the operator  $(I_d + c_r \Omega)$  is not an isometry and will change the length of a generic vector. To show this, let  $x = p_j^* - p_l^*$ . Using the fact that  $\Omega$  is skew-symmetric ( $\Omega^T = -\Omega$ ), the new squared length is:

$$\begin{aligned} \|(I_d + c_r \Omega)x\|^2 &= x^T(I_d - c_r \Omega)(I_d + c_r \Omega)x \\ &= x^T(I_d - c_r^2 \Omega^2)x \\ &= \|x\|^2 - c_r^2 x^T \Omega^2 x = \|x\|^2 + c_r^2 \|\Omega x\|^2. \end{aligned}$$

Since  $\Omega$  is non-zero and  $x$  is a generic vector,  $\|\Omega x\|^2 > 0$ . Therefore, for any  $c_r \neq 0$ , the new squared length is strictly greater than  $\|x\|^2$ , leading to a persistent, non-zero edge error.  $\square$

This result reveals a fundamental dichotomy in the system's response, illustrated in Figures 3 and 4, and discussed in detail in the following subsection.

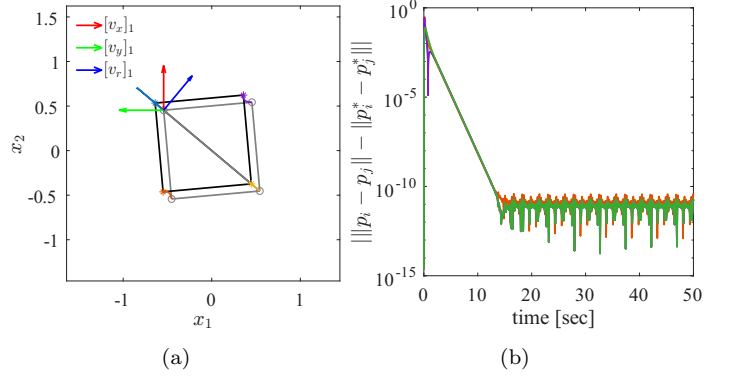


Fig. 3. Shape recovery with an orthogonal input. (a) An impulse orthogonal to the local rotational RBM direction at the actuated node results in a pure translation. (b) The edge length errors decay to zero.

### 5.1 Case Study: Minimally Rigid Framework

To illustrate the shape recovery dichotomy for an infinitesimally rigid framework, we consider a minimally rigid formation of four agents in the plane, as shown in Figures 3 and 4. An impulsive input is applied at node 1.

First, we consider an input  $w_0$  chosen to be orthogonal to the local rotational vector at the actuated node,  $\langle [v_r]_1, w_0 \rangle = 0$ . This corresponds to Case 1 of Proposition 10, which predicts that the rotational mode is not excited ( $c_r = 0$ ). Figure 3(a) shows the resulting motion: the formation undergoes a pure translation. Figure 3(b) confirms this, showing that all edge length errors decay to zero after the initial transient, and the formation perfectly recovers its shape.

Next, we consider an input  $w_0$  that has a component aligned with the local rotational vector,  $\langle [v_r]_1, w_0 \rangle \neq 0$ . This corresponds to Case 2 of the proposition. This input excites the rotational mode ( $c_r \neq 0$ ). Figure 4(a) shows that the final motion is a combination of translation and rotation. This global rotation causes the framework to deform, as shown in Figure 4(b), where the edge length errors converge to persistent, non-zero values. This

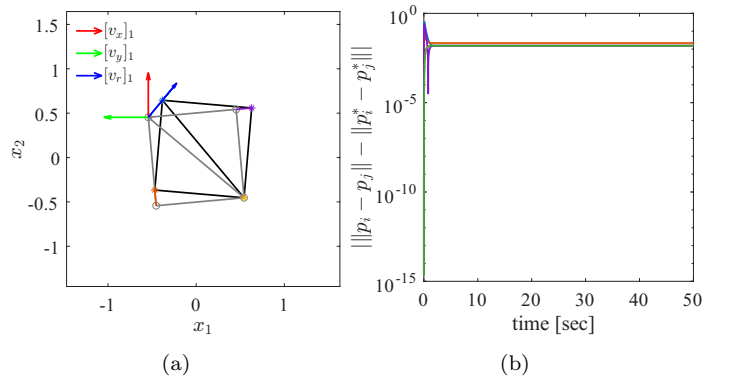


Fig. 4. Shape distortion with an aligned input. (a) An impulse with a component along the local rotational RBM direction excites a rotational motion. (b) The formation deforms, resulting in persistent edge length errors.

simulation provides a clear dynamic validation of our geometric analysis.

The case study demonstrates the shape recovery dichotomy, but a deeper geometric explanation is needed to unify our contributions. The fundamental reason for this behavior lies in the geometry of the mapping from the 2D input space to the 3D space of RBM coordinates. As we will now show, this mapping is constrained in a way that directly explains the dichotomy.

This geometric structure provides the final link between our two main contributions. The mapping from an input  $w_0 \in \mathbb{R}^2$  to the RBM coordinates  $c = (c_x, c_y, c_r) \in \mathbb{R}^3$  is a linear transformation whose image is the “controllable plane” shown in Figure 5. The normal vector to this plane,  $n_c$ , has a direct physical meaning: it is the coordinate vector of the uncontrollable RBM.

To derive this vector, we seek the coordinates of an RBM that is uncontrollable. Let an arbitrary RBM be represented by the coordinate vector  $c = (c_x, c_y, c_r)^\top$ , such that its motion is  $v = c_x v_x + c_y v_y + c_r v_r$ . By Lemma 3, this mode is uncontrollable if and only if its motion at the actuated node is zero,  $v_i = 0$ . This gives the constraint:

$$c_x [v_x]_i + c_y [v_y]_i + c_r [v_r]_i = 0.$$

By choosing a standard basis where  $[v_x]_i = (1, 0)^\top$  and  $[v_y]_i = (0, 1)^\top$ , this simplifies to  $(c_x, c_y)^\top = -c_r [v_r]_i$ . This equation defines a 1D subspace of RBM coordinates. A basis vector for this subspace can be found by setting  $c_r = 1$ , which yields  $(c_x, c_y)^\top = -[v_r]_i$ . This gives the coordinate vector of the uncontrollable RBM as  $n_c = (-[v_r]_i, 1)$ .

The motion corresponding to these coordinates is  $v_{\text{uctrb}} = -[v_r]_{ix} v_x - [v_r]_{iy} v_y + v_r$ , which, as shown previously, corresponds to a motion  $[v_{\text{uctrb}}]_k = [v_r]_k - [v_r]_i$  in the uncontrollable subspace  $\mathcal{R}_i(p^*)$ .

Finally, the fact that any RBM excited by an input  $w_0$  has coordinates  $c = (w_0^\top, \langle [v_r]_i, w_0 \rangle)^\top$  means that it must satisfy the orthogonality condition  $\langle c, n_c \rangle = 0$ . This confines all reachable RBMs to the “controllable plane,” formally defined as the subspace  $\{c \in \mathbb{R}^3 \mid \langle c, n_c \rangle = 0\}$ . This geometric constraint directly explains the shape recovery dichotomy: an input  $w_0$  orthogonal to  $[v_r]_i$  forces  $c_r = 0$ , confining the outcome to the intersection line

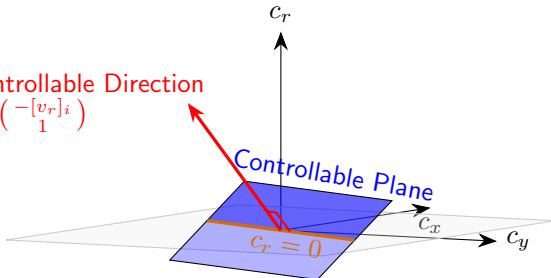


Fig. 5. Geometric illustration of the input-to-RBM map. The set of all reachable RBMs forms the blue “controllable plane.” This plane is orthogonal to the “uncontrollable direction”  $n_c$ . The horizontal plane represents the subspace of pure translations ( $c_r = 0$ ). The intersection of these two planes is the 1D subspace of outcomes that result in perfect shape recovery.

shown in Figure 5. This results in a pure translation and ensures perfect shape recovery.

## 6. CONCLUSION

In this paper, we presented a geometric input-output analysis of hidden modes in distance-based formation control. We proved that for a system with a single actuated agent, the uncontrollable subspace is completely characterized by the local rotational subspace,  $\mathcal{T}_i$ , which contains all motions locally invisible to the controller at the input node  $i$ . This geometric object provides a complete characterization, encompassing both global rigid-body rotations about the input node (the subspace  $\mathcal{R}_i$ ) and locally hidden deformations.

From an input-output perspective, we demonstrated the dynamic consequences of this structure. We proved a shape recovery dichotomy where the system’s ability to reject a localized disturbance is determined by the input’s alignment with the local component of the standard rotational RBM. This input-output link was solidified by showing that the space of all reachable RBMs forms a “controllable plane” whose normal vector is the coordinate representation of the uncontrollable RBM, elegantly unifying the system’s geometric constraints and its dynamic input-output behavior.

While the linearized analysis provides crucial insights, the true system performance is governed by nonlinear effects. Future work will aim to extend our geometric input-output characterization to the original nonlinear dynamics.

## REFERENCES

- Asimow, L. and Roth, B. (1979). The rigidity of graphs, II. *Journal of Mathematical Analysis and Applications*, 68(1), 171–190.
- Babazadeh, R. and Selmic, R. (2019). Distance-based multiagent formation control with energy constraints using sdre. *IEEE Transactions on Aerospace and Electronic Systems*, 56(1), 41–56.
- Chung, S.J., Paranjape, A.A., Dames, P., Shen, S., and Kumar, V. (2018). A survey on aerial swarm robotics. *IEEE Transactions on robotics*, 34(4), 837–855.
- Connelly, R. (2005). Generic global rigidity. *Discrete & Computational Geometry*, 33, 549–563.
- Krick, L., Broucke, M.E., and Francis, B.A. (2009). Stabilisation of infinitesimally rigid formations of multi-robot networks. *International Journal of control*, 82(3), 423–439.
- Oh, K.K. and Ahn, H.S. (2011). Formation control of mobile agents based on inter-agent distance dynamics. *Automatica*, 47(10), 2306–2312.
- Oh, K.K., Park, M.C., and Ahn, H.S. (2015). A survey of multi-agent formation control. *Automatica*, 53, 424–440.
- Olfati-Saber, R. and Murray, R.M. (2002). Distributed cooperative control of multiple vehicle formations using structural potential functions. *IFAC Proceedings Volumes*, 35(1), 495–500. 15th IFAC World Congress.
- Rahmani, A., Ji, M., Mesbahi, M., and Egerstedt, M. (2009). Controllability of multi-agent systems from a graph-theoretic perspective. *SIAM Journal on Control and Optimization*, 48(1), 162–186.

Skogestad, S. and Postlethwaite, I. (2005). *Multivariable Feedback Control: Analysis and Design*. John Wiley & Sons, Inc., Hoboken, NJ, USA.

Tanner, H.G. (2004). On the controllability of nearest neighbor interconnections. In *43rd IEEE Conference on Decision and Control*, volume 3, 2467–2472. IEEE.